

Influence of varying magnet pole-arcs and step-skew on permanent magnet AC synchronous motor performance

Metin AYDIN^{1,*}, Oğuzhan OCAK², Yücel DEMİR³

¹Department of Mechatronics Engineering, Faculty of Engineering, Kocaeli University, Kocaeli, Turkey

²Yektamot Co., Sakarya, Turkey

³Department of Research and Development, MDS Motor Tasarım Ltd., Kocaeli, Turkey

Received: 31.03.2020

Accepted/Published Online: 28.07.2020

Final Version: 30.11.2020

Abstract: Minimization or elimination of cogging torque is a significant issue in permanent magnet (PM) motor design process. There are some design techniques to reduce or eliminate this unwanted torque components in PM motors. This paper focuses on two different design techniques, varying magnet pole-arc and step-skew, to reduce cogging torque component in radial flux PM synchronous motors. Different design points which consider pulsating torque components and back-EMF harmonics are obtained via finite element analysis (FEA) for a low power industrial PM motor. A prototype motor is manufactured for one of the desired designs and is tested experimentally. Good agreement is attained between the analysis and experimental results.

Key words: Permanent magnet motors, servomotors, finite element analysis, cogging torque, torque pulsations, torque ripple

1. Introduction

Permanent magnet (PM) synchronous motors are widely used in industrial applications including home appliances, defense, automotive, servo and robotics due to their high torque/volume-current ratios, compact designs and linear torque speed characteristics [1, 2]. However, one major disadvantage of such motors is pulsating torque if it is not managed during the design stage. This causes many complications such as mechanical vibration, noise, and related problems in the drive systems, which cannot be tolerated in many applications [3–5].

Torque output of a PM motor includes four main components which are namely average torque, reluctance torque, torque ripple, and cogging torque. Average torque is produced by interaction between the field of the rotor and stator current while reluctance torque is caused because of the saliency of the rotor. Furthermore, torque ripple is generated by the field distribution and generated magnetomotive force and the cogging torque is caused by the interaction between magnets and stator slots. If the designed motor is surface mounted PM synchronous motor, reluctance torque component does not arise since there is no difference in d and q-axis reactances. Thus, there are two options to improve the torque quality of surface mounted PM motors: reducing both torque ripple and cogging torque [6].

There exist various methods to reduce or eliminate cogging torque components in PM motors [3–12]. All of these techniques are mainly classified into two main categories: optimization of motor design parameters and

*Correspondence: metin.aydin@kocaeli.edu.tr

current injection. There are various design techniques for reducing cogging torque including magnet shaping and sizing, teeth pairing, minimizing slot openings, adding dummy stator slots, shifting magnets, skewing either stator slots or rotor magnets, selecting coreless and slotless designs [6]. The key design parameter in minimization of torque pulsations is optimizing the magnet geometry which affects both torque ripple and cogging torque components of the motor as well as back-EMF harmonics.

Two different design techniques of minimizing torque pulsations were used in this paper and the best design parameters are found for each design based on cogging components and back EMF harmonics. In the first part, an 8-pole PM motor is designed for a specific application without paying too much attention to torque quality. Both design practices of varying magnet pole-arc and step-skew are applied to the designed rotor in the second part of the paper. All of the design studies are carried out using Flux FEA software by Cedrat¹. Torque components of each method and subsequent back-EMF harmonics are all investigated in detail and design with minimum cogging and minimum voltage harmonic content is completed and summarized. A prototype motor is built based on one of the optimized designs and experimentally verified. Important conclusions are drawn about optimum rotor design with better torque quality and low back-EMF harmonics in the last section of the paper.

2. Definitions of cogging torque and torque ripple for PMAC synchronous motors

A well-known electromagnetic torque equation developed by a PM synchronous motor is given by

$$T = \frac{3}{2}p(\psi_m i_q - (L_q - L_d)i_d i_q), \tag{1}$$

where ψ_m is magnet flux linkage, L_d and L_q are d-q axis inductances, p is pole-pair, and i_d and i_q are d-q axis currents. Since $L_d = L_q$ for surface magnet motors, the torque equation becomes

$$T = \frac{3}{2}p\psi_m i_q. \tag{2}$$

This equation assumes that there exist no cogging or ripple components at the torque output. However, it is inevitable to obtain pulsating torque free motor unless the motor designer takes extra precautions during the design stage to lower or eliminate the pulsating torque components.

Cogging torque occurs as a result of the interaction between magnets on the rotor and slots in the stator. No current excitation is involved in this torque component. Due to its periodic behavior, cogging torque component can be described by using a Fourier series as

$$T_{cog}(\theta_m) = \sum_{k=1}^{\infty} T_k \sin(kN_c \theta_m + \varphi_k), \tag{3}$$

where θ_m is position of the rotor, T_k is the amplitude and φ_k is the phase angle of the k th harmonic, N_c is the least common multiple of the rotor pole number and the stator slots.

Electromagnetic torque ripple caused by the interaction between stator MMF and rotor can be given by [13],

$$T_{rip} = \sum_{n=1}^{\infty} T_{6n} \cos(6n\omega t), \tag{4}$$

¹Cedrat Flux 2D Users Manual. Lyon, France: Cedrat Technologies SA, 2009.

where T_{6n} is harmonic torque components.

The torque ripple factor (TRF), which is an important torque quality measure in PM motors, can be expressed as the ratio of peak-to-peak torque ripple to average torque

$$TRF = \frac{T_{pp}}{T_0} = \frac{2}{T_0} \sqrt{\sum_{n=1}^{\infty} T_{6n}^2}, \quad (5)$$

where T_{pp} is the peak-to-peak electromagnetic ripple torque of the motor, T_0 is the average torque and T_{6n} is harmonic torque components.

Since almost all practical stator windings and PM field distributions have some winding and flux density harmonics, back-EMF waveforms are not perfectly sinusoidal and contain high-order harmonics. As a result, ripple torque exists even with a sinusoidal phase current source. To eliminate this problem, special fractional slot-pole configurations are commonly used in PM motors. However, for integer slot PM motors, some simple and cost effective design methods can be used and torque ripple can be lowered or eliminated at the motor output.

3. Designed permanent magnet motor

FEA is a popular tool in the design of conventional and unconventional electric motors and the development of the available FEA packages has allowed engineers to design PM motors rapidly and efficiency [14, 15]. A design study of an industrial PM motor with 380 V terminal voltage and 4.25 Nm torque at 2500 rpm is carried out with no attention to torque quality. The designed surface mounted motor structure is shown in Figure 1. Motor no-load and on-load flux density variations with flux lines as well as airgap mesh structure are all displayed in Figure 2. Improved mesh density in the motor airgap is achieved using Flux FEA package to increase the accuracy of the finite element calculations. The main parameters of the designed motor are also provided in Table 1. The motor is designed to deliver minimum cogging torque. Therefore, magnet pole-arc is varied in order to find out minimum cogging component. Magnet pole-arc ratio, also called magnet width, is changed from 90 to 165 electrical degrees, and cogging torque simulations are conducted. As seen from Figure 3, peak cogging torque has a minimum value of 0.11 Nm for the magnet pole-arc of 126.25 electrical degrees. This value of cogging torque is nearly 90% lower than the cogging for the pole-arc of 110 degrees electrical and 87% lower than the cogging for the magnet pole-arc of 145 degrees. However, the real drawback of proceeding with such design point is the back-EMF harmonics generated. Figure 4 shows the line back EMF voltages and associated harmonic spectrum at 200 rpm velocity. As seen from the FFT analysis, the line back-EMF voltage has high order harmonics with 5th and 7th being the most significant ones. This could not be acceptable since it generates issues in the drive system. These harmonics will be reflected in the current drawn and will result in extra heating in the stator. In addition, the harmonics will limit the maximum speed of the motor and affect the utilization of the DC bus. Therefore, special attention needs to be given to the elimination of back-EMF harmonics during pulsating torque minimizations.

4. Applied design techniques to reduce torque pulsations

Various design techniques are available to obtain pulsating torque free PM motors [4]. Modifications completed in the stator structure causes manufacturing difficulties and associated cost not to mention additional leakage

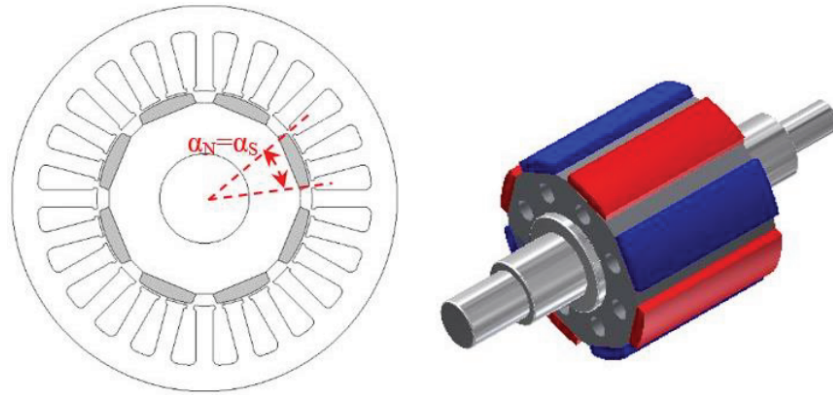


Figure 1. Designed PM AC motor with surface mounted magnets.

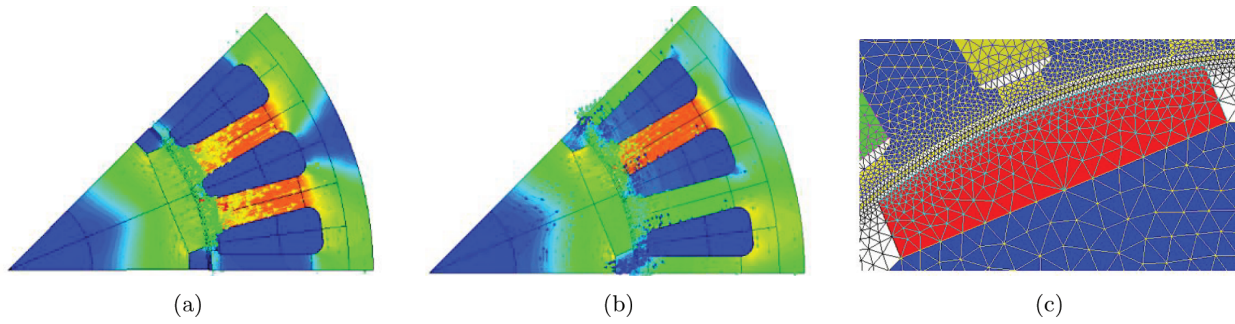


Figure 2. (a) No-load and (b) on-load flux distributions-lines and (c) mesh structure of the designed motor.

Table 1. Parameters of the designed PM motor.

Number of poles	8
Number of slots	24
Rated torque	4.25 Nm
Rated speed	2500 rpm
Airgap	0.5 mm
Slots/pole/phase (q)	1
Magnet type	N35SH
Lamination	M270-50A
Stator OD	91 mm
Stack length	43 mm

components. Thus, design modifications accomplished on the rotor are generally preferred due to simplicity and low cost.

In this study, two different rotor side design techniques are applied to the rotor design and compared with each other: varying magnet pole-arc and stepped rotor. First, a magnet design is completed to obtain minimum cogging torque during the design process of the motor. Then, varying magnet pole-arcs where different magnet pole-arcs are utilized for both N and S poles ($\alpha_N \neq \alpha_S$). This is not very well investigated topic in the

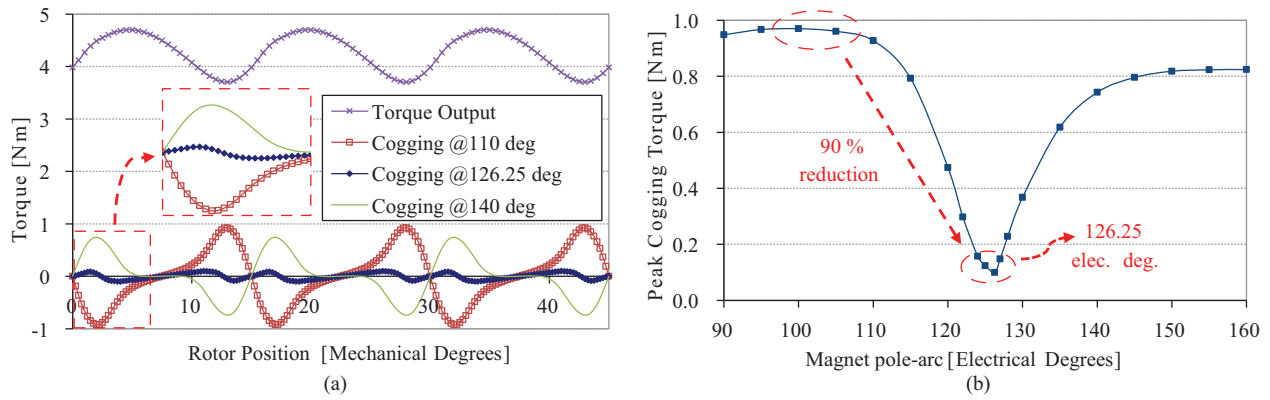


Figure 3. (a) Cogging torque and output torque variations for standard rotor with equal magnet pole-arcs ($\alpha_N = \alpha_S = 126.25$ electrical degrees), and (b) cogging torque peak values for different magnet pole-arcs.

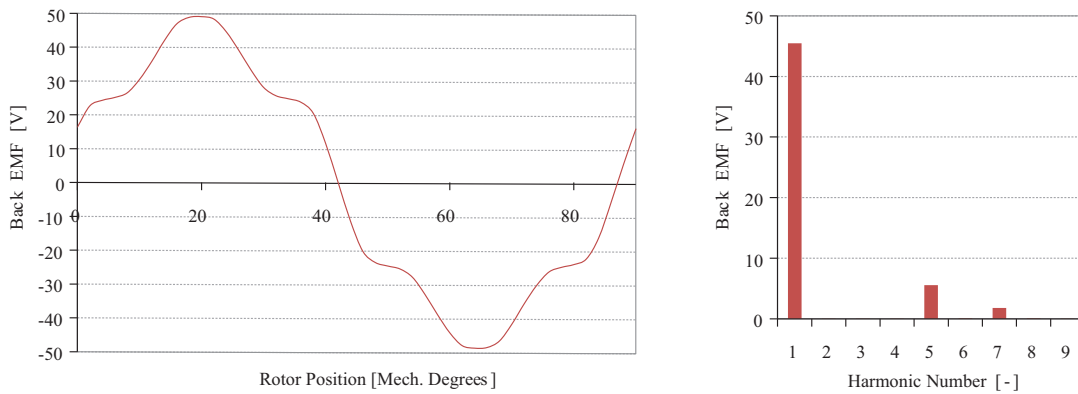


Figure 4. Line voltage and FFT analysis for conventional rotor with equal magnet pole-arcs ($\alpha_N = \alpha_S = 126.25$ electrical degrees).

literature and will be investigated thoroughly in this section. The second method investigated in this study is stepped rotor, also called step-skew, where the rotor is comprised of stepped segments so that a magnet skew is introduced. This method will also be applied to the design and investigated in detail. It should be indicated that both of the design techniques are examined with 2D-FEA.

4.1. Rotor with varying magnet pole-arcs

Using different magnet pole-arcs in rotor is a simple and effective method to minimize torque pulsations in PM motors. Both magnet pole-arcs of N (α_N) and S (α_S) poles are changed independently in this technique as displayed in Figure 5. Figure 6 shows the peak cogging torque levels as a function α_N and α_S , which are adjacent pole-arcs, and shows 2D cogging map. A total of 256 cases with 15616 FEA simulations are conducted to be able to find minimum cogging torque levels by varying both α_N and α_S independently. The analysis took roughly 29 h with good quality mesh structure. The figure clearly shows how the magnet pole-arcs should be in order to minimize the cogging torque. A large plateau of low cogging is observed from the plot and minimum cogging point is obtained for magnet pole-arcs of $\alpha_N = 117.5$ degrees and $\alpha_S = 146.5$ degrees. Peak value of cogging torque becomes 0.11 Nm which is roughly 2.75% of the average torque of the motor.

Figures 7 and 8 show 3D and 2D graphs of 5th and 7th harmonic variations as a function of magnet pole-arcs α_N and α_S respectively. Similar to peak cogging torque graph, the 2D maps are symmetric along the symmetry line. These 3D and 2D plots can allow the designer to find out the design point with either minimum cogging or perfectly sinusoidal back-EMF. When the graphs are examined carefully, it is seen that the intersection of the 2D cogging, 5th and 7th harmonic maps must lead to the optimum design point. Although the design points for minimum cogging and sinusoidal back-EMF are close to each other, the designer must reach a compromise between cogging and sinusoidal back-EMF. In other words, a decision should be made between the manufacturing cost and performance.

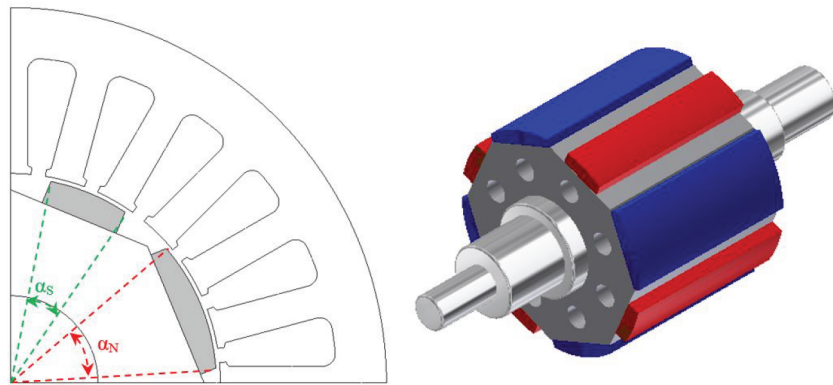


Figure 5. Definition of rotor with varying magnet pole-arcs [α_N describes the pole-arc of (N) magnet and α_S describes the pole-arc of (S) magnet].

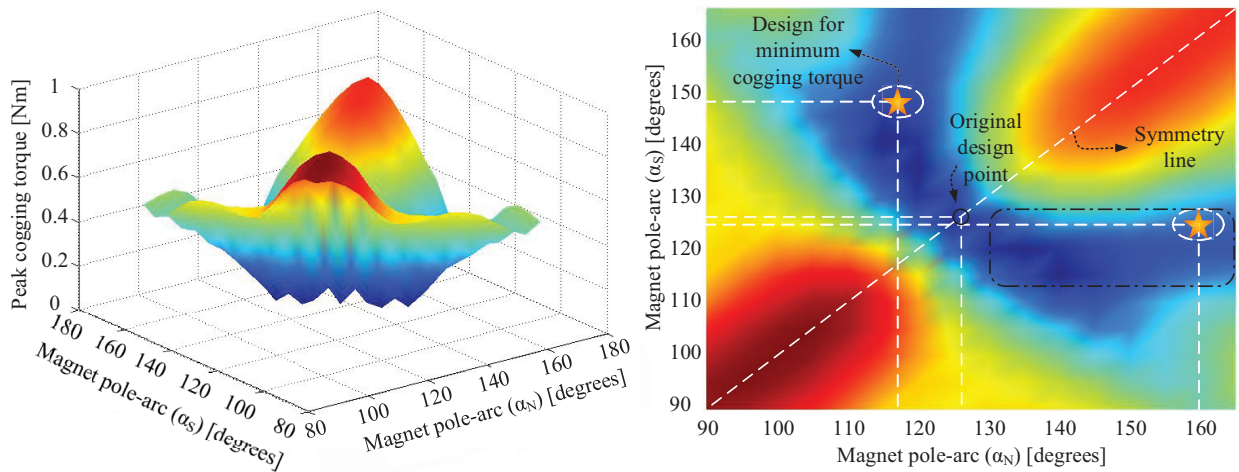


Figure 6. Variation of cogging torque peak values for varying magnet (N and S) pole-arcs: 3D variation and 2D map.

Figures 9 and 10(a) shows cogging torque variation and line back-EMF waveform of both design points. If the motor is designed for optimum cogging point with varying magnet pole-arc, peak cogging is found to be 0.11 Nm. If the design point with harmonic free back-EMF voltages is desired, then the other point must be selected. In addition, as seen from the FFT analyses of both waveforms, 6.0% of 5th harmonic level is observed clearly for the minimum cogging design point. Moreover, Figure 10(b) displays the airgap flux density comparison for

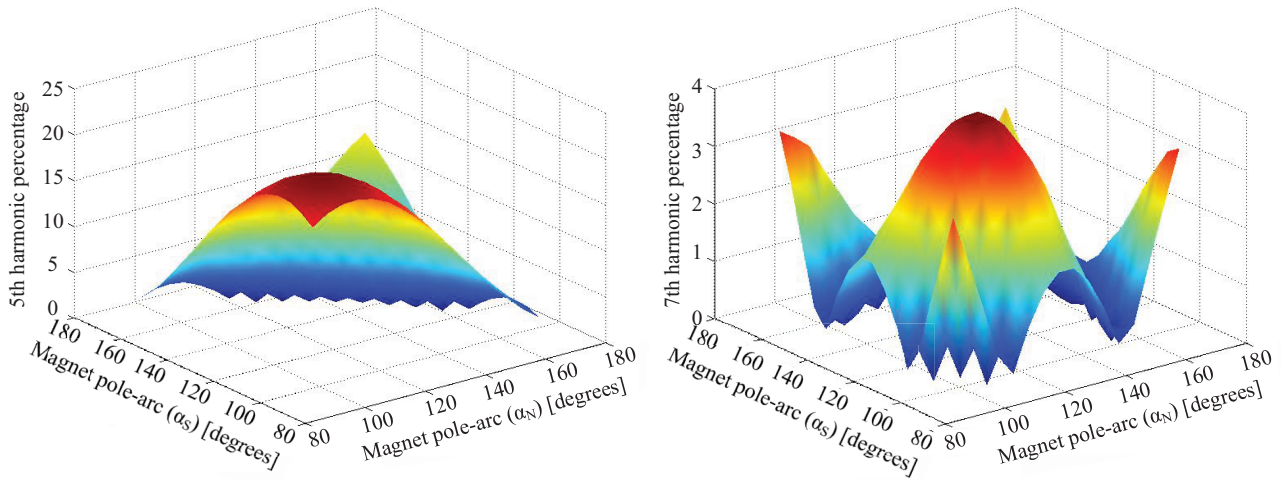


Figure 7. 3D graphs of 5th and 7th harmonics for varying magnet pole-arcs.

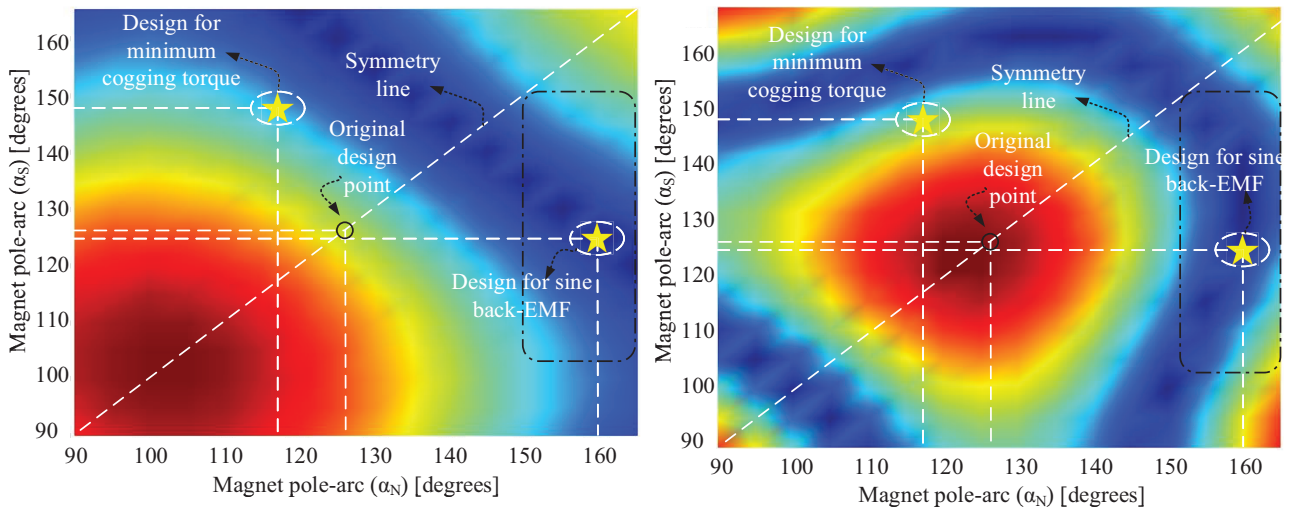


Figure 8. Variation of 5th and 7th harmonics for varying magnet pole-arcs (2D views).

both varying pole-arc design and the original design. Varying pole-arc can help reduce the cogging component dramatically, but can generate subharmonics at the machine airgap which may produce torque ripple at the output. Therefore, careful design strategy has to be followed if this approach is utilized.

4.2. Rotor with step-skew

Step-skew is one of the effective methods to minimize or eliminate cogging components in PM motors. Although it causes manufacturing difficulties and associated cost, it is frequently used in high performance PM motors. The second design technique used in this paper is stepped skew and displayed in Figure 11. Both 2-step and 4-step skew rotors as examples are given in the figure. Using this approach, rotor stack is divided into a number of steps to create skewing effect. Both 2 and 4 stepped skew rotors are applied to this design, and FEA analyses are performed to investigate it.

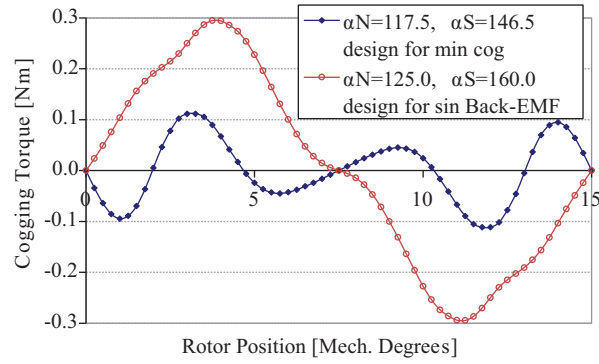


Figure 9. Cogging torque variation for two design points: minimum cogging torque and (lowest THD or) sinusoidal back EMF.

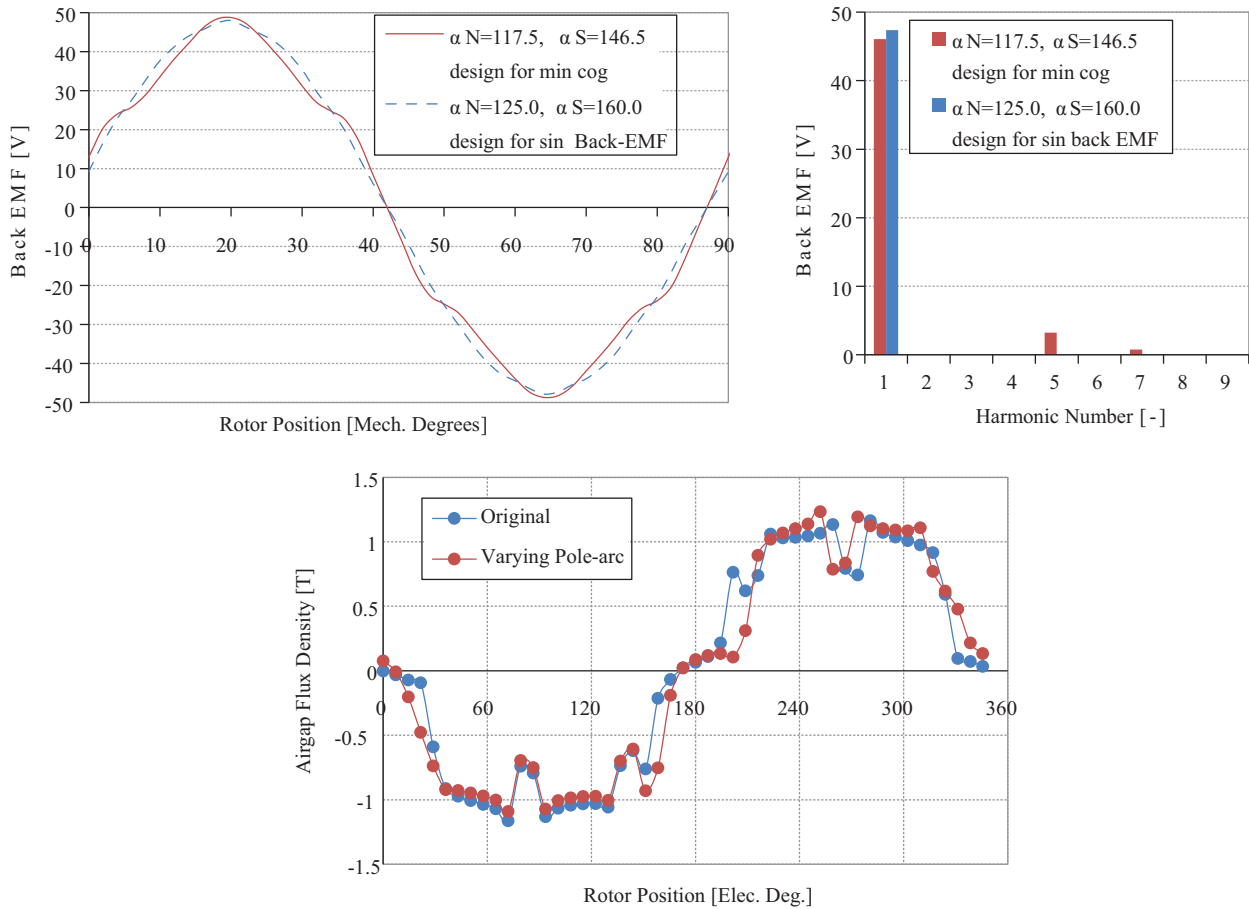


Figure 10. (a) Line voltage (at 200 rpm) and FFT analysis for varying magnet pole-arc: min cogging torque point ($\alpha_N = 117.5$ deg. and $\alpha_S = 146.5$ deg.) and sinusoidal back EMF ($\alpha_N = 160.0$ deg. and $\alpha_S = 125.0$ deg.) and (b) airgap flux density distribution for both designs obtained by FEA.

It is found out that the peak value of minimum cogging torque for 2-step skew rotor is 0.05 Nm. At that point, magnet pole-arc is 155.5 electrical degrees as displayed (Figure 12). At this magnet pole-arc if the rotor

is unsegmented, peak value of cogging torque becomes 0.8 Nm. If 2-step skew is applied in the rotor, cogging torque is reduced by 96% and becomes practically zero. Back-EMF line voltage and its harmonic content are both shown in Figure 13 for 200 rpm angular velocity. As seen from the FFT analysis it has high order harmonics with low harmonic content.

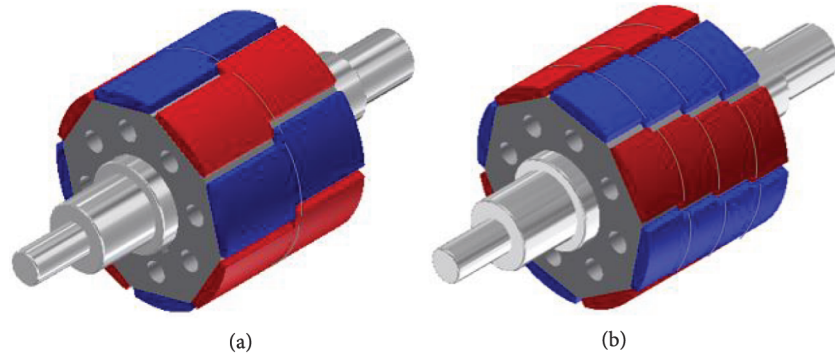


Figure 11. Example for step-skew structures: (a) 2-step-rotor and (b) 4-step-rotor.

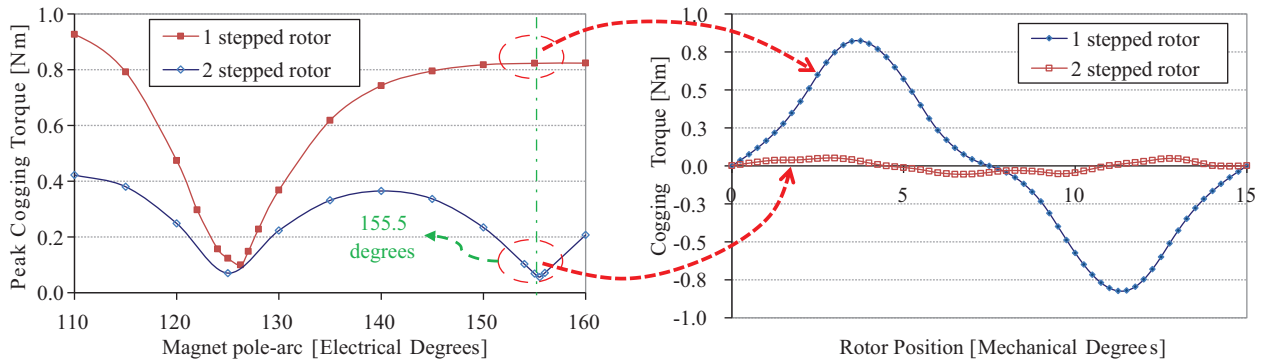


Figure 12. Cogging torque peak values for different magnet pole-arcs and 2 segmented rotor (α_N and α_S), and cogging torque variation for unsegmented and 2 segmented rotor ($\alpha_N = \alpha_S = 155.5$ degrees).

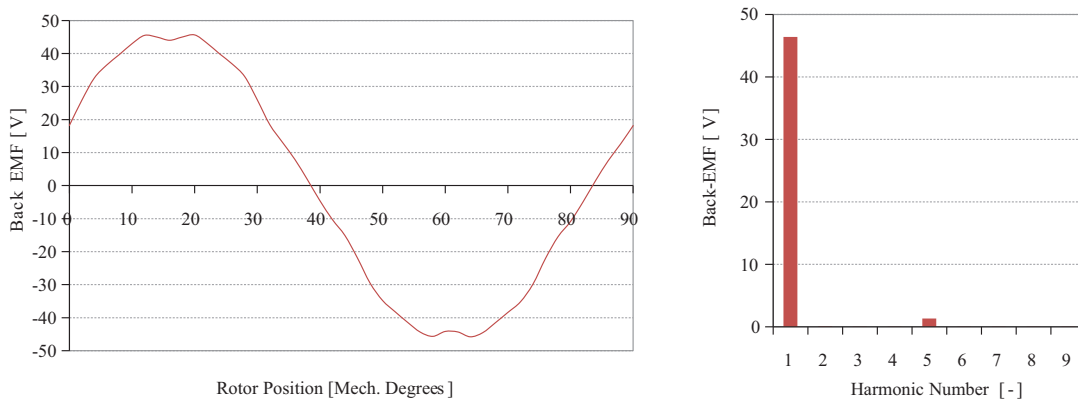


Figure 13. Line back-EMF voltage and FFT analysis for 2 segmented rotor ($\alpha_N = \alpha_S = 155.5$ degrees).

The same analyses are carried out for a 4-step skew rotor which is shown in Figure 11(b). Figure 14 shows the peak value of cogging torque as a function of magnet pitch. It is seen that the peak value of the cogging torque becomes 0.025 Nm with 140 electrical degrees of magnet pole-arc. Back-EMF phase and line voltages are also shown in Figure 15 at 200 rpm rotor angular velocity. As seen from the FFT analysis, line voltage waveform does not include any high order harmonics. Although the manufacturing cost is increased, the low speed motor performance is dramatically improved with the step-skew rotor.

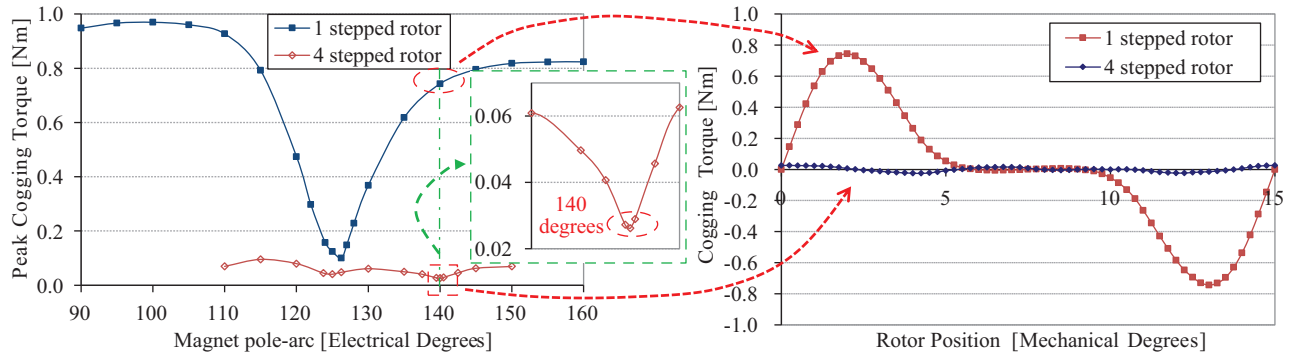


Figure 14. Cogging torque peak values for different magnet pole-arcs and 4 segmented rotor ($\alpha_N = \alpha_S$), and cogging torque variation for unsegmented and 4 segmented rotor ($\alpha_N = \alpha_S = 140$ degrees).

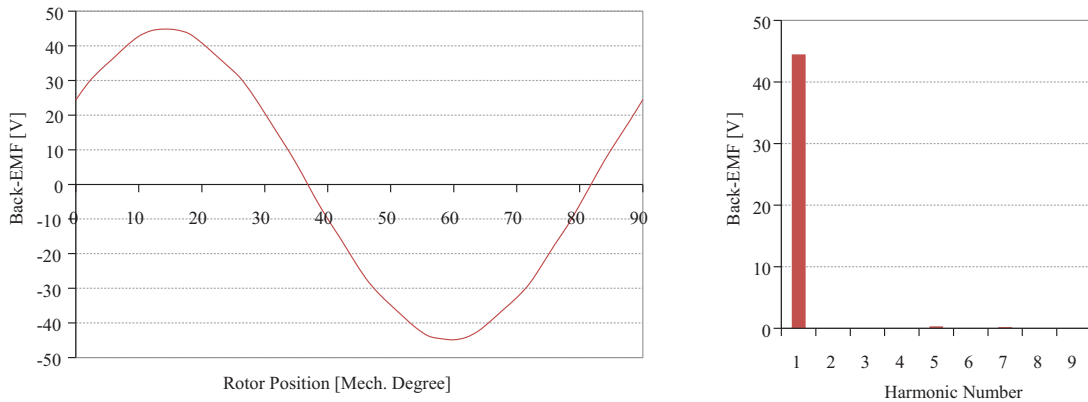


Figure 15. Line back-EMF voltage at 200 rpm and FFT analysis for 4 segmented rotor ($\alpha_N = \alpha_S = 140$ degrees).

5. Pulsating torque component and minimization

Motors with small value of the cogging torque and back-EMF waveforms with harmonic content demonstrate the quality of a PM AC motor. Although magnet pole arc giving minimum cogging is used in the original design point with the same pole-arcs and without stepped rotor, attention has to be paid to induced back-EMF waveforms which has to be harmonics free in order to eliminate torque pulsations. Thus, each rotor design studied in the paper is tested for output torque quality using 2D FEA with the same stator and phase current.

Electromagnetic torque output plots for all of the rotor designs are shown in Figure 16. Design with varying magnet pole arc has better torque output than the original design. Torque ripple of the designed motor is about 23.4% and the torque ripple of the rotor with varying magnet pole-arcs is about 6.1% of the average

torque. 2-step rotor or step-skew rotor has a torque ripple approximately 6.5% and 4-step rotor has minimum torque ripple with 3.5% of the average torque.

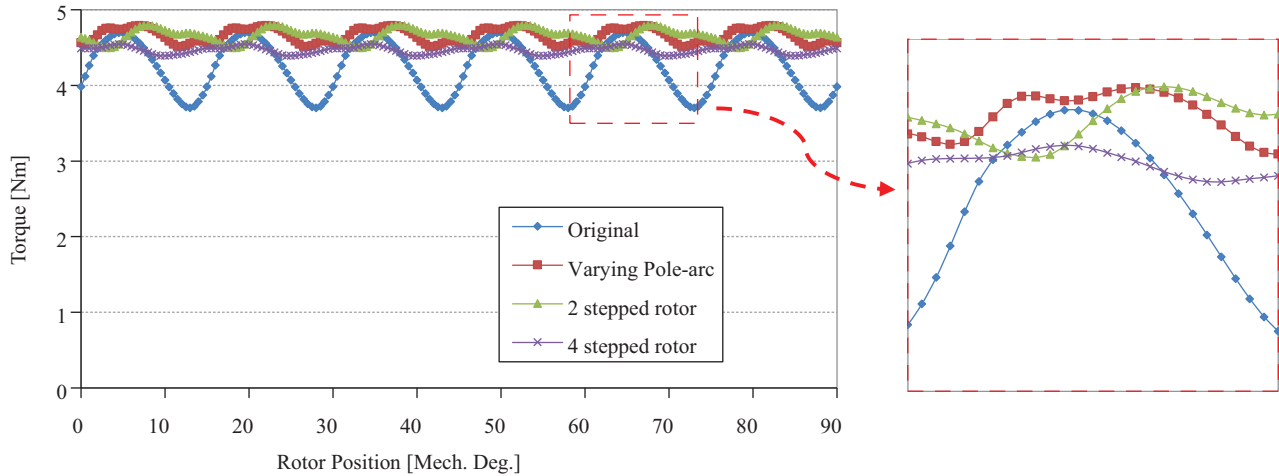


Figure 16. Torque output of standard rotor with equal magnet pole-arcs ($\alpha_N = \alpha_S = 126.25$ degrees), varying magnet pole-arcs ($\alpha_N = 117.5$ degrees and $\alpha_S = 146.48$ degrees), 2-step rotor ($\alpha_N = \alpha_S = 155.5$ degrees) and 4-step rotor ($\alpha_N = \alpha_S = 140$ degrees).

6. Comparison of applied methods and prototype motor

Cogging torque variations for all of the designs are shown in Figure 17. As seen from the figure, segmented rotor structure with 4-step skew offers the minimum cogging torque. At this design, cogging torque peak value is 0.025 Nm which is 75% smaller than the design with varying magnet pole-arc. Furthermore, all four designs are compared in terms of line back-EMF voltages and harmonics obtained at 200 rpm and illustrated in Figure 18. The design with 4 segmented rotor provides very low harmonic content while the other designs have nonsinusoidal back-EMF waveforms arising from either varying magnet pole-arc or 2-step skew.

Torque output comparison is also shown in Figure 19. Design with varying magnet pole-arc, 2-step rotor and 4-step rotor have better torque output than the standard design in terms of torque ripple. Standard design has highest torque ripple/average torque ratio with the value of 23.4% while the others have less than 6.5% torque ripple. All of the average torques and torque ripple values are summarized at Table 2. In addition, Figure 20 shows the comparison of torque-current loci of the designs including the prototype motor.

Table 2. Parameters of the designed PM motor.

	Average torque [Nm]	Cogging torque [%]	Torque ripple or TRF [%]	Magnet volumes [mm^3]
Original rotor	4.25	2.3	23.4	13
Varying magnets	4.66	2.4	6.1	13.4
2-step rotor	4.66	1.1	6.5	15
4-step rotor	4.47	0.58	3.5	14

Although the best design seems to be the 4-step skew rotor, because of the manufacturing costs of segmentation and difficulty in manufacturability, rotor with varying magnet pole-arc with single segmented

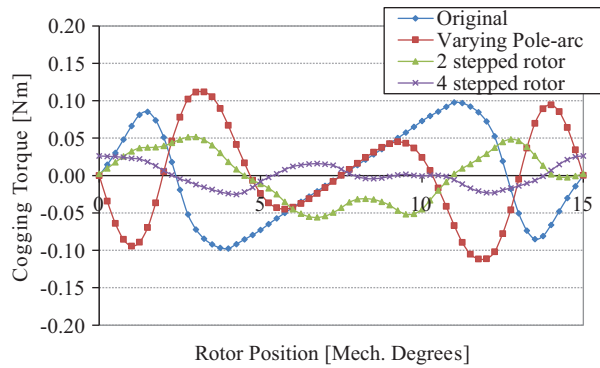


Figure 17. Cogging torque comparison of standard rotor with equal magnets, varying magnet pole-arcs, skewed 2 and skewed 4 segmented rotors.

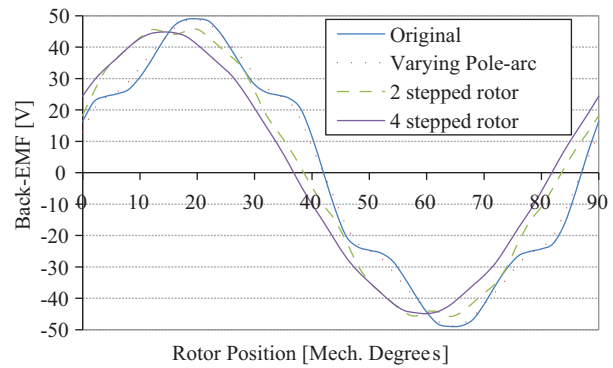


Figure 18. Back-EMF (line voltages) comparison of standard rotor with equal magnets, varying magnet pole-arc, 2 and 4 segmented rotors.

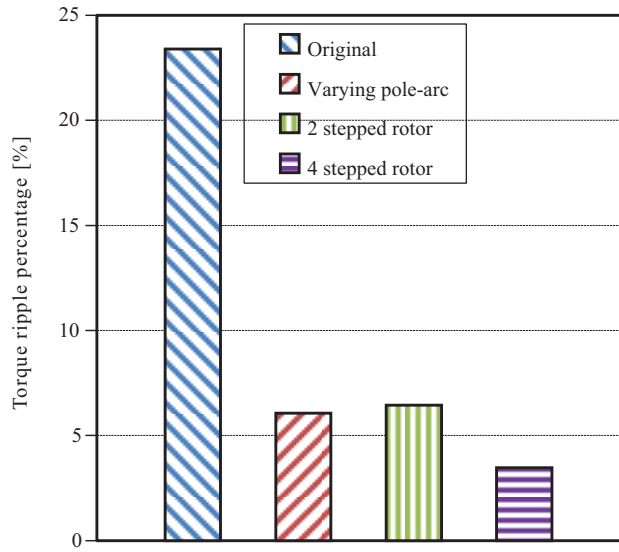
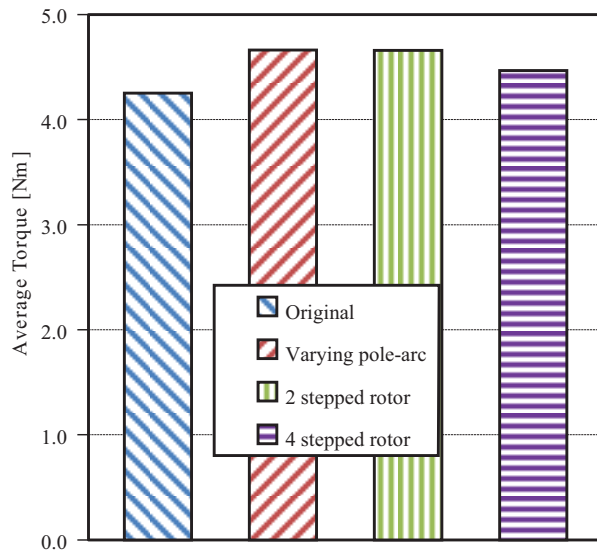


Figure 19. Torque output comparison of standard rotor with equal magnets, varying magnet pole-arc, 2 and 4 segmented rotors.

structure is chosen for building prototype motor. Manufactured motor and its varying rotor magnets are both illustrated in Figure 21.

7. Experimental verification

A test setup is prepared for measuring cogging torque component and back EMF waveforms. Cogging free driving motor and its drive is one of the main components of the experimental set-up. High resolution torque-meter with high sensitivity is also required to measure low cogging torque values accurately. Figure 22 shows the set-up used in this study.

The drive motor is rotated at very low speeds such as 1 rpm for cogging torque measurements and high speeds for back-EMF measurements. Experimental cogging torque data for 60 s and comparison with 2D-FEA are provided in Figure 23. Twenty-four cogging cycles over one mechanical rotation is clearly seen from the

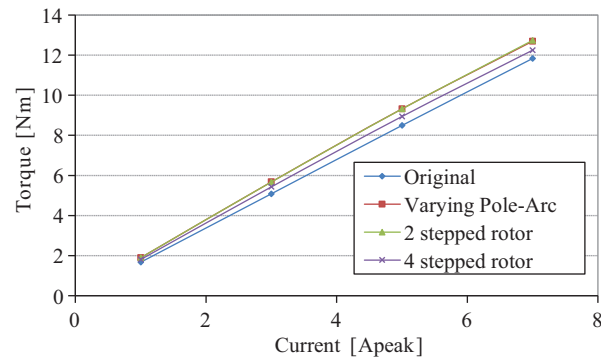


Figure 20. Comparison of torque constants of the designs including the prototype motor.

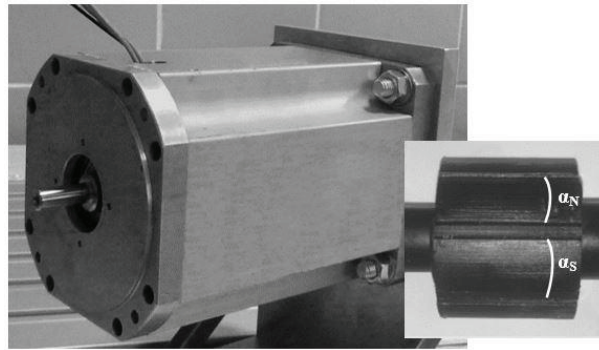


Figure 21. Prototype motor and the rotor structure with varying magnet pole-arc (built for min cogging torque point).

graph. Since this is an integer slot motor with $q = 1$ slot/pole/phase, cogging cycle is 15 mechanical degrees. 0.11 Nm peak cogging torque is found in FEA and good agreement between FEA and experimental results for both peak value and the shape of the cogging torque waveform is observed in the comparison. In addition, the prototype motor is tested to compare the line back-EMF voltages. As seen from Figure 24, 48 V peak line voltage is observed with 6% of the 5th harmonic. Excellent agreement between predicted FEA and experimental results is attained in this study.

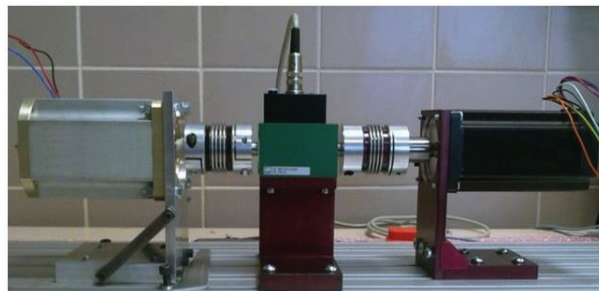


Figure 22. Experimental setup for measuring cogging torque and back-EMF of the prototype motor.

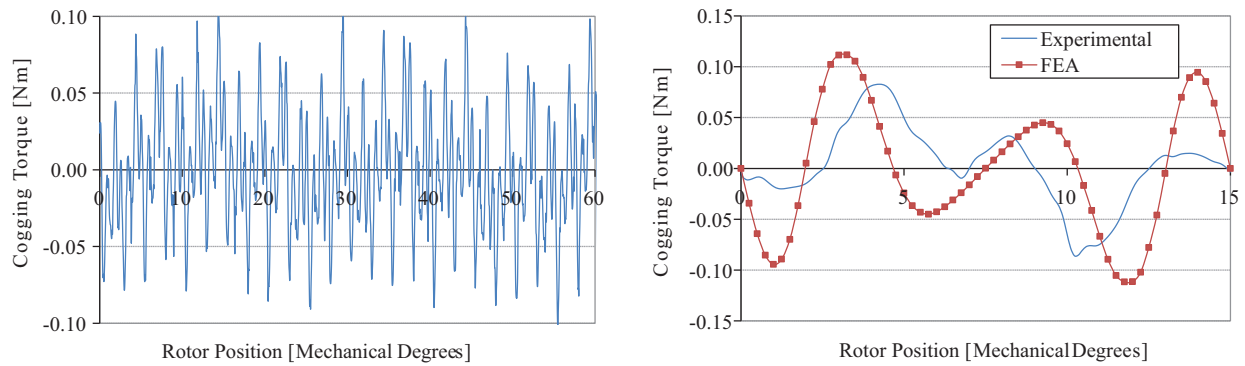


Figure 23. Experimental results of cogging torque component during one rotation and comparison with FEA and test results over one cycle.

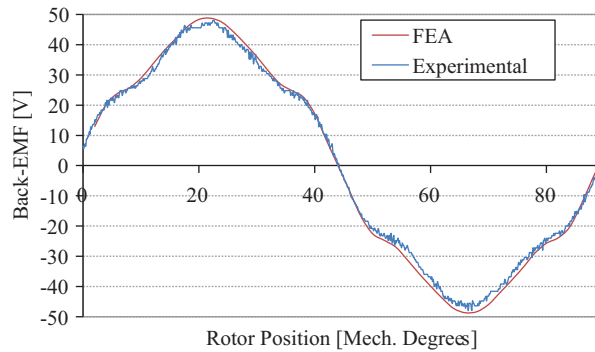


Figure 24. Comparison of line voltages with 2D-FEA and experimental data.

8. Conclusion

Influence of varying magnet pole-arc and step-skew in PM motors in minimizing cogging torque component as well as back-EMF harmonics is investigated in this paper. An integer slot surface mounted PM motor is used in this work. Based on the analyses, rotor with varying magnet pole-arc is the chosen to build the prototype motor and good agreements between the test motor and FEA is obtained. Although using varying magnet pole-arcs increases the magnet manufacturing cost slightly, it helps reduce the cogging torque component significantly for such integer slot combinations. If the rotor design with varying magnet pole-arc is performed thoroughly, design with minimum cogging torque point can be obtained for a particular stator slot combination. Back-EMF harmonics can also be minimized. It has also been shown that step-skew is an effective means of reducing cogging torque component in high performance integer slot PM motors. It also helps reduce the high order back-EMF harmonics and consequently, torque ripple. However, this method requires precise calculation of skew angle and low manufacturing tolerances of the permanent magnets used.

Acknowledgment

This work was supported in part by the Kocaeli University BAP Unit under Grant 2016/77 and MDS Motor Ltd. under Grant No: MDS2018/1-047412 and MDS2017/4-045399.

References

- [1] Hendershot JR, Miller TJ. Design of Brushless Permanent Magnet Motors. Oxford, UK: Clarendon, 1994.
- [2] Dorrell DG, Hsieh MF, Popescu M, Evans L, Staton DA et al. A review of the design issues and techniques for radial-flux brushless surface and internal rare-earth permanent magnet motors. *IEEE Transactions Industrial Electronics* 2011; 58 (9): 3741-3757. doi: 10.1109/TIE.2010.2089940
- [3] Jahns TM, Soong WL. Pulsating torque minimisation techniques for permanent magnet ac motor drives: a review. *IEEE Transactions Industrial Electronics* 1996; 43 (2): 321-330. doi: 10.1109/41.491356
- [4] Bianchi N, Bolognani S. Design techniques for reducing the cogging torque in surface-mounted PM motors. *IEEE Transactions on Industry Applications* 2002; 38 (5): 1259-1265. doi: 10.1109/TIA.2002.802989
- [5] Kang GH, Son YD, Kim GT, Hur J. A novel cogging torque reduction method for interior-type permanent-magnet motor. *IEEE Transactions Industry Applications* 2009; 45 (1): 161-167. doi: 10.1109/TIA.2008.2009662
- [6] Islam R, Husain I, Fardoun A, McLaughlin K. Permanent-magnet synchronous motor magnet design with skewing for torque ripple and cogging torque reduction. *IEEE Transactions Industry Applications* 2009; 45 (1): 152-160. doi: 10.1109/TIA.2008.2009653
- [7] Zhu ZQ, Howe D. Influence of design parameters on cogging torque in permanent magnet machines. *IEEE Transactions Energy Conversion* 2000; 15 (4): 407-412. doi: 10.1109/60.900501
- [8] Dosiek L, Pillay P. Cogging torque reduction in permanent magnet machines. *IEEE Transactions Industry Applications* 2007; 43 (6): 1565-1571. doi: 10.1109/TIA.2007.908160
- [9] Li T, Slemon G. Reduction of cogging torque in permanent magnet motors. *IEEE Transactions on Magnetics* 1988; 24 (6): 2901-2903. doi: 10.1109/20.92282
- [10] Wang D, Wang X, Kim M, Jung S. Integrated optimization of two design techniques for cogging torque reduction combined with analytical method by a simple gradient descent method. *IEEE Transactions on Magnetics* 2012; 48 (8): 2265-2276. doi: 10.1109/TMAG.2012.2191416
- [11] Ge X, Zhu ZQ, Kemp G, Moule D, Williams C. Optimal step-skew methods for cogging torque reduction accounting for three-dimensional effect of interior permanent magnet machines. *IEEE Transactions on Energy Conversion* 2017; 32 (1): 222-232. doi: 10.1109/TEC.2016.2620476.
- [12] Wang X, Sun X, Gao P. Study on the effects of rotor-step skewing on the vibration and noise of a PMSM for electric vehicles. *IET Electric Power Applications* 2020; 14 (1): 131-138. doi: 10.1049/iet-epa.2019.0238
- [13] Aydin A, Huang S, Lipo TA. Torque quality and comparison of internal and external rotor axial flux surface-magnet disc machines. *IEEE Transactions Industrial Electronics* 2006; 53 (3): 822-830. doi: 10.1109/TIE.2006.874268
- [14] Ionel DM, Popescu M. Finite element surrogate model for electric machines with revolving field—application to IPM motors. *IEEE Transactions Industry Applications* 2010; 46 (6): 2424-2433. doi: 10.1109/TIA.2010.2073671
- [15] Ionel DM, Popescu M. Ultra-fast finite element analysis of brushless PM machines based on space–time transformations. In: *IEEE International Electric Machines and Drives Conference*; Miami, FL, USA; 2009.